α Structures for $A = 4N$ Nuclei in the $2s$-$1d$ Shell*

Paul S. Hauge and S. A. Williams
Institute for Atomic Research and Department of Physics, Iowa State University, Ames, Iowa 50010
and
George H. Duffey
Department of Physics, South Dakota State University, Brookings, South Dakota 57006
(Received 18 June 1971)

The classical α-particle model has been consistently applied to all $4N$ nuclei in the $2s$-$1d$ shell. The ^{20}Ne nucleus was found to be a D_{2d} distorted tetrahedron in agreement with earlier investigations. Electron scattering form factors were predicted, but there are at present no experimental data for comparison. Most interesting results were obtained for ^{24}Mg, where the experimental matrix elements, energy spectrum, and electron scattering form factors were found to definitely favor a D_{2h} bitetrahedron over the D_{4h} square bipyramid used in other papers. Recent experiments on ^{28}Si also slightly favor an oblate D_{3d} structure over the previously considered D_{5h} pentagonal bipyramid. No definite structures could be established for ^{32}S and ^{36}Ar, because of the large number of α particles involved. However, a unique structure was found for ^{40}Ca. It consists of six α clusters arranged in an octahedron outside of a tetrahedral ^{16}O core.

I. INTRODUCTION

Any postulated nuclear structure that contains transient or permanent α clusters may be called an α-particle model. Because of the different possibilities, various types of calculations[1] are based on such models. The α-particle model has never enjoyed the success of the shell or collective models, but much evidence accumulated mainly during the last 15 years now strongly suggests α clustering for many light nuclei.[2-11] Arguments have been made for assuming that these α clusters are quite isolated[2,3]; consequently, a few theories have been developed which deal only with the relative motions of the α clusters.[4] In the present paper, we will consider only the simplest of these theories; it is completely phenomenological and applies only to light $A = 4N$ nuclei. Sometimes referred to as the classical α-particle (CAP) model,[5] it assumes that the internal α particles are harmonically bound in a semirigid molecular structure. The observed properties are then predicted by methods analogous to those used in molecular mechanics and are found to depend primarily on the symmetry of the assumed structure.

Since it was first formulated in 1937,[2] the CAP model has yielded reasonably good agreement with the experimental energy levels, electron scattering form factors, and reduced matrix elements for $1p$-shell nuclei.[6-9] Early applications of the model to $4N$ nuclei in the $2s$-$1d$ shell assumed that the α clusters were arranged in a bipyramidal configuration, with all but two of the α particles forming a regular polygon in the equatorial plane. These structures were thought to be the most stable of all possible configurations because they contained the greatest number of bonds between adjacent α particles.[12] However, recent calculations of the electron scattering form factors using these bipyramidal shapes have shown that they are in rather poor agreement with experiment.[13,14] Furthermore, nonbipyramidal forms have been shown to give better agreement with the observed energy levels.[15,16] Since the time of these calculations, much additional experimental information has been obtained; so it was felt that all configurations for the $4N$ nuclei in the $2s$-$1d$ shell should be reconsidered. This paper presents the results from such research.

In Sec. II, we describe the necessary theory, and the results for various nuclei are given in Sec. III. Some general results concerning the charge and mass shapes of many light $4N$ nuclei are then reported in Sec. IV. Finally, in Sec. V we summarize the most important results, concluding that the CAP model works well for only the lower half region of the $2s$-$1d$ shell.

II. THEORY

Energy Spectrum

The CAP model considers only collective motion of the α clusters, so the most general Hamiltonian to be considered is that of the semirigid asymmetric rotor vibrator for n particles[17]:

$$H = H_{\mathrm{rot}} + H_{\mathrm{vib}}, \tag{1}$$

where

$$H_{\mathrm{rot}} = \sum_{j=1}^{3} A_j L_j^2 = \frac{A_1 + A_2}{2}(L^2 - L_3^2) + \frac{A_1 - A_2}{2}(L_+^2 + L_-^2) + A_3 L_3^2, \tag{2}$$

and

$$H_{\rm vib} = \sum_{i=1}^{3n-6} (n_i + \tfrac{1}{2})\hbar\omega_i \,. \tag{3}$$

In Eq. (2), $A_j = \hbar^2/2I_j$, I_j is the moment of inertia with respect to the jth-body fixed axis and the L_j are the usual angular momentum operators with $L_\pm = \mp\sqrt{\tfrac{1}{2}}(L_1 \pm iL_2)$. In Eq. (3), $\hbar\omega_i$ is the energy of the ith normal vibration.

Since $H_{\rm rot}$ and $H_{\rm vib}$ are uncoupled, the eigenfunctions of H have the form

$$\langle \Omega, Q_i | L^\pi MN; n_i\rangle = \sum_K a^L_{NK} \left(\frac{2L+1}{8\pi^2}\right)^{1/2} D^{L\pi *}_{MK}(\Omega) \times \prod_{i=1}^{3n-6} H_{n_i}(Q_i)\,, \tag{4}$$

where the expansion coefficients a^L_{NK} must satisfy certain symmetry relationships because of the invariance of $H_{\rm rot}$ under the operations of D_{2h}.[17] In particular, the sum on K is over either even or odd values of K, $|K| \leq L$, while Ω refers to the three Euler angles that specify the instantaneous orientation of the body-fixed axes with the space-fixed coordinate system. Also in Eq. (4), $H_{n_i}(Q_i)$ is the n_ith Hermite function in the ith normal coordinate, and N is an ordinal number that distinguishes the rotational levels having the same L value. Parity is attached to the rotational wave functions of Eq. (4), since we consider point groups of the full rotation group (rotations plus reflections).

For later use, we note that the expansion coefficients a^L_{NK} depend upon only one parameter, namely $(A_1 - A_2)/(2A_3 - A_1 - A_2)$. This fact may be most easily seen by rewriting Eq. (2) as

$$H = \frac{(A_1 + A_2 + A_3)}{3} L^2 + \frac{(2A_3 - A_1 - A_2)}{6} \times \left[(2L_3{}^2 - L_1{}^2 - L_2{}^2) + \frac{3(A_1 - A_2)}{(2A_3 - A_1 - A_2)} (L_1{}^2 - L_2{}^2) \right]. \tag{5}$$

Any wave function that diagonalizes the square-bracketed term in Eq. (5) also diagonalizes H. The wave function of this bracketed term depends only upon $(A_1 - A_2)/(2A_3 - A_1 - A_2)$, while the factor $\frac{1}{6}(2A_3 - A_1 - A_2)$ serves as a scale factor for the energy spectrum and $\frac{1}{3}(A_1 + A_2 + A_3)L^2$ is merely an additive constant (for fixed L). This fact will be used later in the calculation of electron scattering form factors.

For most of our calculations the rotor is that of a symmetric top, i.e., $A_1 = A_2$. In this limit, $|K|$ becomes a good quantum number replacing the ordinal label, and the Hamiltonian simplifies to

$$H = A_1 L(L+1) + K^2(A_3 - A_1) + H_{\rm vib}. \tag{6}$$

The eigenfunctions of H in this case are independent of the rotational parameters (A_j's), being usually of the form

$$\langle \Omega, Q_i | L^\pi MK; n_i\rangle = \left(\frac{(2L+1)(1+\delta_{K0})}{16\pi^2}\right)^{1/2} \times [D^{L\pi *}_{MK}(\Omega) \pm D^{L\pi *}_{M,-K}(\Omega)]\Psi_{\rm vib}(Q_i)\,. \tag{7}$$

In each configuration studied, the nucleons are assumed to form persistent α clusters of a definite point group symmetry. As a consequence, H is invariant under all operations of this point group carried out in the body-fixed coordinate system, and each $\Psi_{\rm vib}$ and $\Psi_{\rm rot}$ must form a basis function for one of the irreducible representations (IR) of the point group.[18] In addition to leaving H invariant, the operations of this point group will also merely permute identical bosons (α particles). Statistics thus allow only those wave functions of Eqs. (4) or (7) to occur which are symmetric under all operations of the group. This symmetry will exist only if $\Psi_{\rm rot}$ and $\Psi_{\rm vib}$ belong to the same IR. If no normal vibration is excited, both $\Psi_{\rm rot}$ and $\Psi_{\rm vib}$ must belong to the completely symmetric IR of the group.

One can readily find which wave functions belong to each IR by using standard group theoretical techniques.[15-20] The rotational wave functions are classified in Table I for all point groups used in this paper. Normal modes for each structure can be found by standard means[20] and are tabulated later for each nucleus. The lowest-lying experimental rotational bands of a nucleus presumably are built on the zero-point normal vibrations and must therefore be correlated with the theoretical K^π bands associated with the completely symmetric IR's which are given at the top of each column in Table I. Using this assumption, one can usually eliminate all but one of the possible structures for each nucleus. One can then further verify this remaining structure by identifying higher observed states with rotational states built on normal vibrations. Of the seven point groups listed in Table I, six refer to symmetric-top structures. The only one that is associated with an asymmetric top is the D_{2h} point group.

While the symmetry of the assumed structure dictates the quantum numbers of the allowed states, the spacing between levels is determined by the rotation and vibration parameters. The Hamiltonian, Eq. (1) or (6), does not include rotation-vibration interactions; but these should mainly affect the level spacing by effectively reducing the rotational parameters whenever a normal vibration is excited.[17] We attempt to account for these interactions only by changing the rotational parameters

TABLE I. Allowed rotational K^π bands for each IR (denoted Γ) of various point groups. Unless otherwise stated, all energy levels with $L \geq K$ are allowed for each band. Note that parity is conserved within each IR only if the point group includes the inversion operation.

Γ	D_{2d} K^π bands	Γ	D_{2h} K^π bands	Γ	D_{3d} K^π bands	Γ	D_{3h} K^π bands	Γ	D_{4d} K^π bands	Γ	D_{4h} K^π bands	Γ	D_{5h} K^π bands
A_1	0^+ (L even), $2^-, 4^+, \cdots$	A_g	0^+ (L even), $2^+, 4^+, \cdots$	A_{1g}	0^+ (L even), $3^+, 6^+, \cdots$	A_1'	0^+ (L even), $3^-, 6^+, \cdots$	A_1	0^+ (L even), $4^-, 8^+, \cdots$	A_{1g}	0^+ (L even), $4^+, 8^+, \cdots$	A_1'	0^+ (L even), $5^-, 10^+, \cdots$
B_1	0^- (L even), $2^+, 4^-, \cdots$	A_u	0^- (L even), $2^-, 4^-, \cdots$	A_{1u}	0^- (L even), $3^-, 6^-, \cdots$	A_1''	0^- (L even), $3^+, 6^-, \cdots$	B_1	0^- (L even), $4^+, 8^-, \cdots$	A_{1u}	0^- (L even), $4^-, 8^-, \cdots$	A_1''	0^- (L even), $5^+, 10^-, \cdots$
A_2	0^+ (L odd), $2^-, 4^+, \cdots$	B_{1g}	0^+ (L odd), $2^+, 4^+, \cdots$	A_{2g}	0^+ (L odd), $3^+, 6^+, \cdots$	A_2'	0^+ (L odd), $3^-, 6^+, \cdots$	A_2	0^+ (L odd), $4^-, 8^+, \cdots$	A_{2g}	0^+ (L odd), $4^+, 8^+, \cdots$	A_2'	0^+ (L odd), $5^-, 10^+, \cdots$
B_2	0^- (L odd), $2^+, 4^-, \cdots$	B_{1u}	0^- (L odd), $2^-, 4^-, \cdots$	A_{2u}	0^- (L odd), $3^-, 6^-, \cdots$	A_2''	0^- (L odd), $3^+, 6^-, \cdots$	B_2	0^- (L odd), $4^+, 8^-, \cdots$	A_{2u}	0^- (L odd), $4^-, 8^-, \cdots$	A_2''	0^- (L odd), $5^+, 10^-, \cdots$
E	$1^\pm, 3^\pm, 5^\pm, \cdots$	B_{2g}	$1^+, 3^+, 5^+, \cdots$	E_g	$1^+, 2^+, 4^+, \cdots$	E'	$1^-, 2^+, 4^+, \cdots$	E_1	$1^+, 3^-, 5^-, \cdots$	B_{1g}	$2^+, 6^+, 10^+, \cdots$	E_1'	$1^-, 4^+, 6^+, \cdots$
		B_{2u}	$1^-, 3^-, 5^-, \cdots$	E_u	$1^-, 2^-, 4^-, \cdots$	E''	$1^+, 2^-, 4^-, \cdots$	E_2	$2^\pm, 4^\pm, 6^\pm, \cdots$	B_{1u}	$2^-, 6^-, 10^-, \cdots$	E_1''	$1^+, 4^-, 6^-, \cdots$
		B_{3g}	$1^+, 3^+, 5^+, \cdots$					E_3	$1^-, 3^+, 5^+, \cdots$	B_{2g}	$2^+, 6^+, 10^+, \cdots$	E_2'	$2^+, 3^-, 7^-, \cdots$
		B_{3u}	$1^-, 3^-, 5^-, \cdots$							B_{2u}	$2^-, 6^-, 10^-, \cdots$	E_2''	$2^-, 3^+, 7^+, \cdots$
										E_g	$1^+, 3^+, 5^+, \cdots$		
										E_u	$1^-, 3^-, 5^-, \cdots$		

somewhat for each normal vibration. It should be emphasized that it is possible to obtain good agreement with experiment by using one set of average rotational parameters for all vibrations as has been done in previous papers.[6,15,16] However, by allowing some variation in these parameters, we can obtain better agreement with experiment and also study the variation of the effective rotational parameters with changing normal vibrations.

Electron Scattering Form Factors

The charge distribution of the nucleus for the CAP model is given by

$$\rho(\vec{r}, \vec{\mathrm{R}}_i) = 2e \sum_{i=1}^{n} \rho_0(|\vec{r} - \vec{\mathrm{R}}_i|), \tag{8}$$

where $\rho_0(r)$ is the charge density of each α particle normalized to unity, n is the number of α clusters, and $\vec{\mathrm{R}}_i$ is the position of the ith α particle. A derivation of the differential electron scattering cross section using Eq. (8) and the Born approximation is sketched in Ref. 13. In our notation, the formula for scattering from the 0^+ ground state to an excited L_N^π state is

$$\left(\frac{d\sigma}{d\Omega}\right)_{LN}^{\pi} = \left(\frac{d\sigma}{d\Omega}\right)_{\text{point}}^{\pi} |F_{LN}^{\pi}|^2, \tag{9}$$

where $(d\sigma/d\Omega)_{\text{point}}$ is the well-known Mott scattering formula,[21] and the form factor F_{LN}^{π} is given by

$$F_{LN}^{\pi} = \sqrt{4\pi}\, \frac{F_\alpha}{n} \sum_K a_{NK}^L \sum_{i=1}^{n} j_L(qR_i) Y_{LK}(\hat{R}_i). \tag{10}$$

In Eq. (10) q is the momentum transfer of the scattered electron and F_α is the form factor for each α cluster. In the next section, explicit form factors are calculated for several symmetric-top structures. Since $|K|$ is then a good quantum number, the form factor of Eq. (10) will be denoted by F_{LK}^{π}.

Most of the calculations in this paper will involve small momentum transfer ($q \lesssim 3$ fm^{-1}). In this limit $\rho(r)$ can be approximated as a Gaussian function, and F_α becomes

$$F_\alpha = e^{-q^2a^2/6}, \tag{11}$$

where a is the rms radius of each α cluster. The interactions between α clusters may cause their rms radii to be slightly larger than the 1.63 fm valid for the ^{4}He nucleus.[22] Indeed, in our calculations, the parameter a was found to lie between 1.7 and 2.0 fm.

Electric Transition Matrix Elements

Intrinsic electric multipole moments are calculated in the long-wavelength approximation by the

formula

$$E_{lm}=\left(\frac{4\pi}{2l+1}\right)^{1/2}\int d^3r\, r^l \rho(r) Y_{lm}(\hat{r}), \tag{12}$$

where $\rho(r)$ is the nuclear charge density defined by Eq. (8). Since this formula is obtained by considering only the fields outside the nucleus, we can picture the charge of each spherical α particle as being concentrated at its center of mass. The integration thus yields

$$E_{lm}=2e\left(\frac{4\pi}{2l+1}\right)^{1/2}\sum_{i=1}^{n} R_i^l Y_{lm}(\hat{R}_i), \tag{13}$$

an expression independent of the rms radius of each α cluster.

The reduced transition probabilities are the same as for the collective model and are given by[21]

$$B[E(l); L'N' \to LN]=\frac{1}{2L'+1}|\langle L'N'\|E(l)\|LN\rangle|^2, \tag{14}$$

where from the Wigner-Eckart theorem[23] one obtains

$$\langle L'N'\|E(l)\|LN\rangle$$

$$\equiv\frac{[(2l+1)/4\pi]^{1/2}\langle L'N'M'|\sum_{m'} D^{l*}_{mm'}(\Omega)E_{lm'}|LNM\rangle}{(-)^{L'-M'}\begin{pmatrix} L' & l & L \\ -M' & m & M\end{pmatrix}}$$

$$=\left[\frac{(2L'+1)(2l+1)(2L+1)}{4\pi}\right]^{1/2}\times\sum_{\substack{K,K'\\ m}}(-)^{L'+K'}a^L_{N'K'}a^L_{NK}E_{lm'}\begin{pmatrix} L' & l & L \\ -K' & m' & K\end{pmatrix}. \tag{15}$$

In Eq. (15), the multipole moments are assumed to be given in the adiabatic approximation. Since we shall only consider transitions between states with the same vibrational mode, this should be a reasonably good approximation.

All configurations used in this paper will be either symmetric or slightly asymetric tops (i.e., $A_1 \approx A_2$). With this assumption, one can readily find the approximate quadrupole shapes of these nuclei. The second and third columns of Table II give experimental matrix elements, each of which can be used to calculate a theoretical intrinsic quadrupole moment (given in columns 4 and 5). The necessary relationship follows from Eq. (15) using $a^L_{NK}=\delta_{K0}$. The result is

$$Q_{20}\equiv 2E_{20}=\left(\frac{16\pi}{5(2L'+1)(2L+1)}\right)^{1/2}\times\langle L'\|E(2)\|L\rangle\Big/\begin{pmatrix} L' & 2 & L \\ 0 & 0 & 0\end{pmatrix}. \tag{16}$$

Also shown, in column 6, is the experimental ratio $B(E2, 4^+ \to 2^+)/B(E2, 2^+ \to 0^+)$. Discrepancies between these values and the theoretical ratio of 10/7 (for the symmetric top) indicate that collective vibrations or single-particle effects are of some importance in these low-lying states and help explain the slightly different answers obtained in columns 4 and 5. Nevertheless, the results definitely show that ^{20}Ne, ^{24}Mg, and ^{32}S are highly prolate, while ^{28}Si is oblate. This information is of great help in formulating structures for these nuclei.

III. RESULTS FOR VARIOUS NUCLEI (REF. 24)

^{20}Ne

The experimental spectrum of ^{20}Ne shows a definite $K^\pi = 2^-$ band beginning at 4.97 MeV. As has been noted previously,[16] the only rigid α structure

TABLE II. Values for the intrinsic quadrupole moment of various nuclei as calculated from two different reduced matrix elements.

Nucleus	Experimental reduced matrix elements (e fm^2) $\langle 2\|\|E(2)\|\|2\rangle$	$\|\langle 0\|\|E(2)\|\|2\rangle\|$	Corresponding intrinsic quadrupole moments, Q_{20} (fm^2) (From column 2)	(From column 3)	Experimental $\frac{B(E2, 4^+ \to 2^+)}{B(E2, 2^+ \to 0^+)}$
^{20}Ne	-32 ± 4 [a]	19.7 ± 1.0 [a]	$+84 \pm 11$	$\pm 62.5 \pm 3.2$	0.8 ± 0.2 [b]
^{24}Mg	-33 ± 5 [c, d]	24.6 ± 2.7 [e]	$+87 \pm 12$	$\pm 78.0 \pm 8.6$	0.7 ± 0.3 [b]
^{28}Si	$+21 \pm 5$ [f-h]	19.1 ± 0.5 [e]	-54 ± 14	$\pm 60.6 \pm 1.6$	0.9 ± 0.3 [b]
^{32}S	-26 ± 8 [f]	14.6 ± 0.9 [e]	$+70 \pm 21$	$\pm 46.3 \pm 2.6$	2.6 ± 0.7 [i]

[a] K. Nakai, F. S. Stephens, and R. M. Diamond, Nucl. Phys. A150, 114 (1970).
[b] J. H. Anderson and R. C. Ritter, Nucl. Phys. A128, 305 (1969).
[c] O. Häusser, B. W. Hooton, D. Pelte, T. K. Alexander, and H. C. Evans, Phys. Rev. Letters 22, 359 (1969).
[d] A. Bamberger, P. G. Bizzeti, and B. Povh, Phys. Rev. Letters 21, 1599 (1968).
[e] Reference 30.
[f] K. Nakai, J. L. Québert, F. S. Stephens, and R. M. Diamond, Phys. Rev. Letters 24, 903 (1970).
[g] D. Pelte, O. Häusser, T. K. Alexander, B. W. Hooton, and H. C. Evans, Phys. Letters 29B, 660 (1969).
[h] O. Häusser, T. K. Alexander, D. Pelte, B. W. Hooton, and H. C. Evans, Phys. Rev. Letters 23, 320 (1969).
[i] Reference 34.

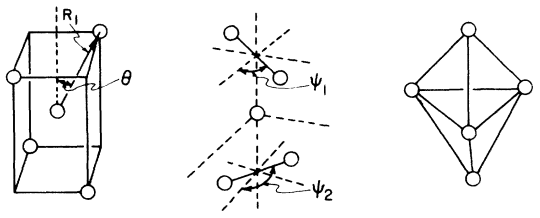

(a) D_{2d} DISTORTED TETRAHEDRON (b) D_{2d} INTERNAL ROTATOR (c) D_{3h} TRIGONAL BIPYRAMID

FIG. 1. (a)–(c) Some of the possible configurations for ^{20}Ne.

that can predict this band is the D_{2d} distorted tetrahedron [Fig. 1(a)]. But in this model, the upper and lower dumbbell structures are separated by a relatively large distance, so they can rotate about the z axis in opposite directions. The amount of such motion would depend upon the height and width of the potential barrier opposing free internal rotation. So, besides reviewing the results of the D_{2d} distorted tetrahedron, we will account for this "tunneling" effect[6,25] by considering the more realistic nonrigid structure of Fig. 1(b). The most popular α structure for ^{20}Ne has been the D_{3h} trigonal bipyramid[5,13,18,25,26] of Fig. 1(c). Since this structure incorrectly predicts a low-lying $K^\pi = 3^-$ band (c.f., Table I), it will not be considered further.

Figure 2 compares the predicted levels of the D_{2d} distorted tetrahedron with experiment. Since this structure is that of a symmetric top, the exact formulas for the rotational energies may be taken from Eq. (6). The symmetries of the nine intrinsic normal vibrations are given in Table III along with the calculated energies and rotational parameters for the vibrations believed to be observed in the experimental spectrum. In some cases, only a lower limit is given for A_3. The parameter A_3 must be at least this large in order to push certain theoretical levels that are not experimentally observed above 10 MeV.

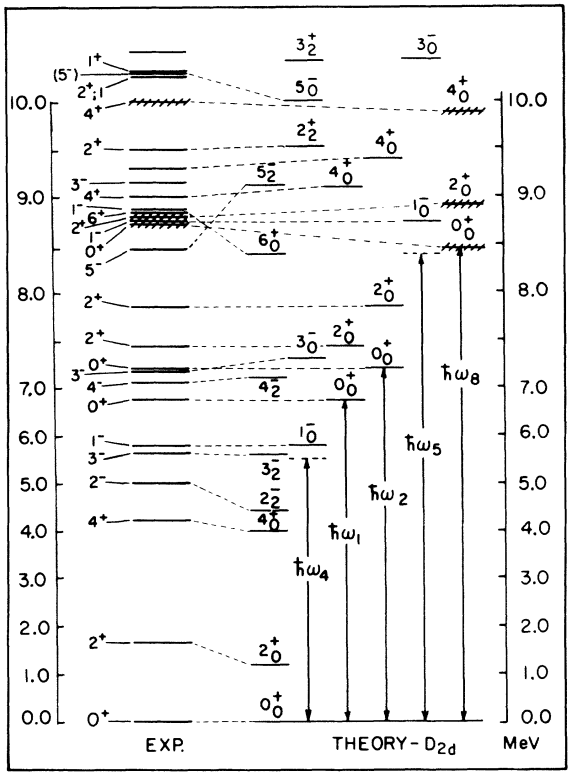

FIG. 2. Comparison of experimental levels of ^{20}Ne with theoretical levels predicted from the D_{2d} structure. The levels built on the zero-point vibrational mode can be better predicted if different values of A_1 are assigned for the $K=0$ and $K=2$ bands. Note that the scale is changed at 7 MeV for clarity.

Nearly all levels below 10 MeV are well explained as rotational states built on the allowed normal vibrations. The explicit K^π bands have long been known; indeed, our level assignments are similar to those arising from other collective models.[27] The third $K=0^+$ band beginning at approximately 8.7 MeV is built on a double vibration of ω_4. This interpretation is supported by the high reduced α

TABLE III. Possible normal vibrations for the D_{2d} distorted tetrahedron structure of ^{20}Ne. The symmetry of the double vibration is found by taking the direct product $B_2 \otimes B_2$.

Frequency	···	ω_1	ω_2	ω_3	ω_4	ω_5	ω_6	ω_7	$\omega_8 \simeq 2\omega_4$
Irreducible representation	A_1	A_1	A_1	B_1	B_2	B_2	E	E	$A_1 = B_2 \otimes B_2$
Observed energy of excitation (MeV)	0	6.7	7.2	···	5.5	8.4	≈9.0	···	≈8.5
Rotational parameters (MeV)									
$A_1 = A_2$	0.20	0.12	0.11	···	0.15	0.17	···	···	0.07
A_3	1.0	≥0.76	≥0.64	···	0.93	≥0.32	···	···	

widths (≈1300 keV) observed for levels of this band.[28] The excitation energy of this vibration should be somewhat less than $2\hbar\omega_4$ because of anharmonic terms in the potential. The lowest levels observed but not predicted are 1^- and 3^- levels around 9 MeV. These levels might be accounted for if we assume that they belonged to the doubly degenerate E vibrational mode. But one would then have several other states in this region which are apparently not observed. Naturally, the 2^+, $T=1$ level at 10.27 MeV cannot be explained, since the CAP model predicts only states with isospin zero.

Besides the two doubly degenerate E vibrations, the only normal mode not observed is the B_1 "twisting" vibration which describes the possible oscillations of the two dumbbells about the z axis. This mode is denoted ω_3 in Table III, and is characterized by a low-lying rotational spectrum of $L_K^\pi = 0_0^-, 2_0^-, 4_0^-, \ldots$. One can understand why this vibration is not observed by considering the hindered internal rotor of Fig. 1(b). If no potential barrier exists between the two dumbbells, the rotational Hamiltonian and wave function can be written as[17,29]

$$H_{\rm rot} = A_1[L(L+1) - K^2] + 2A_3 m_1^2 + 2A_3 m_2^2 , \qquad (17)$$

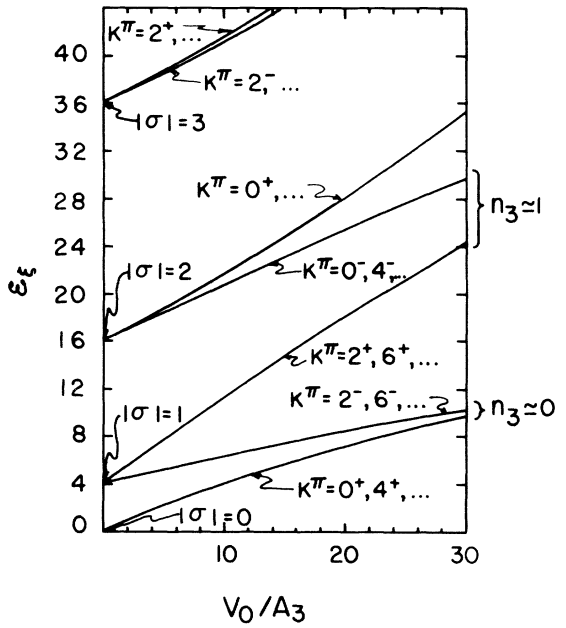

FIG. 3. The part of the energy that depends on the internal rotation, $\mathcal{E}_\xi$, is plotted as a function of V_0/A_3. The correlation between torsional oscillation and free rotation is explicitly shown. The quantities A_3 and V_0 can be uniquely determined from the experimental positions of the first $K=2$ bands. Bose statistics allow only certain K^π bands to be built on each level.

and

$$\langle \varphi\theta\psi_1\psi_2 | LM; m_1 m_2 \rangle = e^{iM\varphi} d^L_{MK}(\theta) e^{im_1\psi_1} e^{im_2\psi_2} . \qquad (18)$$

In these equations m_1 and m_2 are the angular momenta of each dumbbell about the body-fixed z axis, while the $2A_3$ of Eq. (17) comes from the fact that the moment of inertia about the z axis of each dumbbell is $\frac{1}{2}$ that of the total structure. By defining

$$\psi = \tfrac{1}{2}(\psi_1 + \psi_2), \quad K = m_1 + m_2 ,$$
$$\alpha = \psi_2 - \psi_1 , \quad \sigma = \tfrac{1}{2}(m_2 - m_1) , \qquad (19)$$

one can rewrite Eqs. (17) and (18) as

$$H_{\rm rot} = A_1 L(L+1) + K^2(A_3 - A_1) + 4A_3\sigma^2 , \qquad (20)$$

and

$$\langle \varphi\theta\psi; \alpha | LMK; \sigma \rangle = e^{iM\varphi} d^L_{MK}(\theta) e^{iK\psi} e^{i\sigma\alpha} \equiv D^{L*}_{MK}(\Omega) e^{i\sigma\alpha} , \qquad (21)$$

where α denotes the internal angle between the two dumbbells. Statistics now require the wave function to be invariant under $\psi_1 \to \psi_1 + \pi$ and $\psi_2 \to \psi_2 + \pi$. This forces m_1 and m_2 to be even integers or, equivalently, K to be even, and σ to be integral.

In analogy to molecular calculations,[29] we now introduce a suitable interaction between the two dumbbells and rewrite Eq. (20) as

$$H_{\rm rot} = A_1 L(L+1) + K^2(A_3 - A_1) - 4A_3 \frac{d^2}{d\alpha^2} + V_0 \cos^2\alpha . \qquad (22)$$

The last term has minima at $\alpha = \pm 90^\circ$ and represents the potential barrier that each dumbbell must tunnel through in order for the structure to go from a right- to a left-handed system. The wave functions are now of the form

$$\langle \Omega; \alpha | LMK; \xi \rangle \sim D^{L*}_{MK}(\Omega) M_\xi(\alpha) . \qquad (23)$$

The $M_\xi(\alpha)$'s are Mathieu functions with the following limiting properties:

$$\lim_{V_0 \to 0} M_\xi(\alpha) \to e^{\pm i\sigma\alpha} ,$$
$$\lim_{V_0 \to \infty} M_\xi(\alpha) \to H_{n_3}(Q_3) , \qquad (24)$$

where Q_3 represents the "twisting" mode previously considered. The energies are easily found by diagonalizing the Hamiltonian in Eq. (22) among the free-rotor wave functions of Eq. (21). The resultant energy can be written as

$$E_{LK\xi} = A_1 L(L+1) + K^2(A_3 - A_1) + A_3 \mathcal{E}_\xi\left(\frac{V_0}{A_3}\right), \qquad (25)$$

where the last term is plotted in Fig. 3.

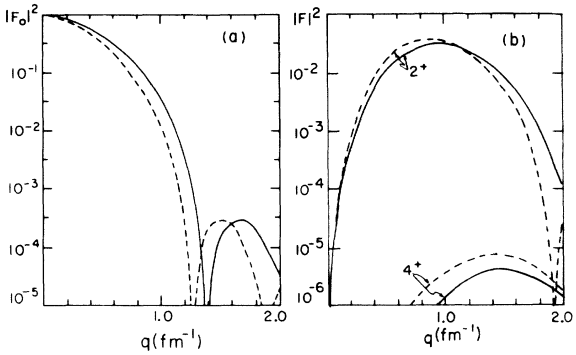

FIG. 4. Theoretical cross sections for ^{20}Ne: (a) elastic scattering form factors, (b) inelastic scattering form factors for the 2^+ (1.63 MeV) and the 4^+ (4.25 MeV) states. Solid line represents $a_0 = 1.9$ fm, $a = 1.7$ fm, $R_1 = 2.65$ fm. From similar calculations on ^{28}Si, we expect centripetal distortion to alter the parameters somewhat for the excited states. The dashed line represents the same parameters except $R_1 = 3.0$ fm and should give a better fit to the $L^\pi = 2^+$ state. In Fig. 4(b) θ is taken to be 30°.

From this figure, one sees that this tunneling effect alters only the K^π bands of ω_3, pulling the $K^\pi = 2^+$ band far below the 0^- band for reasonable values of V_0. The value of V_0 could be estimated from the experimental separation energy of the $K^\pi = 2^-$ and $K^\pi = 2^+$ bands. Since no $L^\pi = 3^+$ states are observed under 10 MeV, the $K^\pi = 2^+$ band cannot start lower than the $L^\pi = 2^+$ state at 9.5 MeV (c.f., Fig. 2), and this fact implies a separation energy of at least 4.5 MeV. By careful examination of Fig. 3, we can then conclude that $V_0 \geq 10$ MeV and 0.7 MeV $\leq A_3 \leq 1.0$ MeV. It should be noted that only two or three of the 20 states observed at present below 10 MeV are of unnatural parity. Thus it is conceivable that an $L^\pi = 3^+$ state at approximately 8 MeV may be unobserved. If this were true, it would definitely lower our value for V_0.

Unfortunately, no detailed electron scattering experiments have been performed for ^{20}Ne. Such experiments would help determine the exact charge shape of the nucleus. For the D_{2d} configuration, simple forms for the form factors (denoted F^π_{LK}) may be found from Eqs. (10) and (11) and Fig. 1(a). These expressions for scattering to the lowest three levels are

$$F^+_{00} = \tfrac{1}{5}F_\alpha[1 + 4j_0(qR_1)],$$

$$F^+_{20} = \tfrac{4}{5}\sqrt{5}\,F_\alpha P_2(\cos\theta) j_2(qR_1),$$

and

$$F^+_{40} = \tfrac{12}{5}F_\alpha P_4(\cos\theta) j_4(qR_1). \quad (26)$$

These same equations also hold for the hindered internal rotor of Fig. 1(b). In Fig. 1(a), R_1 and θ are defined. In analogy with ^{28}Si, for which the form factors have been measured, we expect the four outer α clusters to increase the radius of the inner one slightly. If this effect is included in our calculations, only the elastic form factor is changed, becoming

$$F^+_{00} = \tfrac{1}{5}[e^{-q^2a_0^2/6} + 4e^{-q^2a^2/6} j_0(qR_1)], \quad (27)$$

where a_0 is the rms radius of the center α particle. The theoretical absolute squares of the form factors are plotted in Fig. 4. From results on ^{28}Si (which will be considered shortly), we choose R_1, a_0, and a to be 2.65, 1.9, and 1.7 fm, respec-

TABLE IV. Comparison of theoretical and experimental values for certain transitions in ^{20}Ne. The values for the two parameters are $|Q_{20}| = 58.3$ fm^2 and $|E_{32}| = 27.3$ fm^2.

Initial state energy L^π (MeV)	Final state energy L^π (MeV)	Type of transition	Transition rate $\|M^2\|$ (in Weisskopf units) Experiment	Theory
2^+ 1.63	0^+ 0.0	$E2$	24.2 ± 2.5 [a]	21.0
4^+ 4.25	2^+ 1.63	$E2$	16.2 ± 2.8 [a]	30.0
6^+ 8.79	4^+ 4.25	$E2$	28.0 ± 6.0 [a]	33.0
8^+ 11.99	6^+ 8.79	$E2$	...	34.6
2^- 4.97	0^+ 0.0	$M2$	0.002 [b]	...
	2^+ 1.63	$E1$	$7.4^{+2.1}_{-1.9} \times 10^{-6}$ [c]	0.0
		$M2$	0.017 [b]	...
		$E3$	$5.8^{+5.1}_{-3.5}$ [b]	12.5
3^- 5.63	0^+ 0.0	$E3$	7^{+3}_{-2} [b]	5.0
	2^+ 1.63	$E1$	$4.7^{+1.3}_{-0.8} \times 10^{-6}$ [c]	0.0
		$M2$	...	...
		$E3$	<3.0 [b]	0.0
4^- 7.02	2^+ 1.63	$M2$	≤ 0.14 [b]	...
		$E3$	≤ 6.0 [b]	6.7

[a] K. Nakai, F. S. Stephens, and R. M. Diamond, Nucl. Phys. A150, 114 (1970).
[b] C. Broude, A. E. Litherland, R. W. Ollerhead, and T. K. Alexander, Can. J. Phys. 45, 3837 (1967).
[c] H. C. Evans, M. A. Eswaran, H. W. Gove, and A. E. Litherland, Can. J. Phys. 43, 82 (1967).

tively, for elastic scattering; but we expect R_1 to increase to 3.0 fm for inelastic scattering because of centripetal distortion. We assume a reasonable value for θ of 30°. Of particular interest is the form factor for the 4^+ level which is very sensitive to the choice of θ. Indeed, the theoretical cross section $|F_{40}^+|^2$ increases by a factor of 10^2 if θ is changed by ±5° [since $P_4(\cos\theta)$ goes through one of its zeros at $\theta = 30.6°$]. With $R_1 = 2.65$ fm and $\theta = 30°$, the intrinsic electric moments are calculated to be $Q_{20} = 70.2$ fm^2 and $|E_{32}| = |E_{3-2}| = 44.2$ fm^3. With $\theta = 25°$, the results change to $Q_{20} = 81.9$ fm^2 and $|E_{32}| = |E_{3-2}| = 32.9$ fm^3. The quadrupole moments compare favorably with Table II.

Table IV compares experimental transitions of low-lying states with those predicted by the structure. The values for the two parameters are taken to be $|Q_{20}| = 58.3$ fm^2 and $|E_{32}| = |E_{3-2}| = 27.3$ fm^3 which are fairly close to those indicated in the previous paragraph.

^{24}Mg

The α structure usually assumed for ^{24}Mg is the D_{4h} square bipyramid shown in Fig. 5(a). All low-lying levels can be accounted for if one assumes the $K^\pi = 2^+$ band beginning at 4.23 MeV is built on a normal vibration belonging to the B_{1g} IR of D_{4h} (c.f., Table I). However, a low-lying $K^\pi = 0^+$ band is predicted but not observed at around 4 MeV.[18] Also this configuration gives a poor fit to the electron scattering data and predicts a negative intrinsic quadrupole moment[14] contrary to the results given in Table II.

Reviewing the other possible configurations, we find that a structure with D_{2h} symmetry, which has not been considered before, will also account for the same energy levels, and further with one less parameter. Also, the $K^\pi = 2^+$ band is not then built on a vibration, and one can give explicit expressions for the electron scattering form factors of these states as was not done in the D_{4h} case. There are two possible nonplanar structures with this symmetry [Fig. 5(b, c)]. Although both structures predict the same energy spectrum, the bitetrahedron [Fig. 5(c)] is found to be in better agreement with the experimental electron scattering form factors and so should be the correct structure. Other possible configurations have been eliminated previously.[16] The calculation of the energy levels for this structure is like that for the asymmetric rotor of Davydov and Fillipov,[21] since both models have the same spatial symmetry (D_{2h}). In fact, the existence of this particular α structure might explain why the asymmetric rotor works well in ^{24}Mg, but not for ^{20}Ne or ^{28}Si.

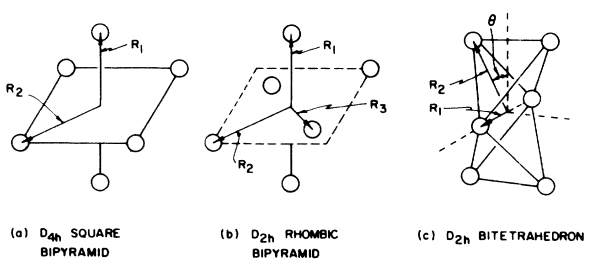

FIG. 5. (a)–(c) Some of the possible structures for ^{24}Mg along with the parameters that can be varied to fit experimental data.

Table I lists the rotational quantum numbers for each IR of D_{2h}. Since a D_{2h} structure constitutes an asymmetric rotor, the energies must be found by diagonalizing the Hamiltonian in Eq. (2) among all rotational wave functions of the same L and same D_{2h} symmetry. For the pure rotational spectrum, it proved more convenient to vary three new parameters uniquely determined by the A_j. These parameters are the rotational energies of the first two $L^\pi = 2^+$ states (denoted E_2 and $E_{2'}$) and a parameter γ which determines the wave functions of these two states in the form

$$\langle \Omega | 2^+ M\rangle = \left(\frac{5}{8\pi^2}\right)^{1/2}\{\cos\gamma D^{2*}_{M0}(\Omega) + \sqrt{\tfrac{1}{2}}\sin\gamma[D^{2*}_{M2}(\Omega) + D^{2*}_{M-2}(\Omega)]\}, \tag{28}$$

$$\langle \Omega | 2'^+ M\rangle = \left(\frac{5}{8\pi^2}\right)^{1/2}\{-\sin\gamma D^{2*}_{M0}(\Omega) + \sqrt{\tfrac{1}{2}}\cos\gamma[D^{2*}_{M2}(\Omega) + D^{2*}_{M-2}(\Omega)]\}.$$

The relations between these three parameters and the three rotational parameters are

$$\begin{aligned} &A_1 + A_2 + A_3 = \tfrac{1}{4}(E_2 + E_{2'}),\\ &2A_3 - A_1 - A_2 = \tfrac{1}{2}\cos 2\gamma(E_{2'} - E_2),\\ &\sqrt{3}(A_2 - A_1) = \tfrac{1}{2}\sin 2\gamma(E_{2'} - E_2). \end{aligned} \tag{29}$$

Figure 6 is a graph of the rotational energies built on the zero-point vibrational state. Both E_2 and $E_{2'}$ are fixed by experiment, and γ is allowed to vary between ±90°. The periodicity of the levels in γ shows that these energies are symmetric under the six permutations of the A_j. Only those experimental levels of ^{24}Mg associated with the zero-point vibrational mode are shown. Good results are obtained only for the redundant values $\gamma \approx 0$, ±60°; consequently ^{24}Mg is very nearly a prolate symmetric top as assumed in Table II. Figure 5(c) is drawn with $A_3 > A_1 \approx A_2$; so we limit the asymmetry parameter to $|\gamma| \leq 10°$.

The rotation-vibration interactions were found to affect the energy levels just enough to make it

virtually impossible to determine γ more accurately than already given. Thus, for simplicity, we set $\gamma = 0°$ and calculate the energy levels of ^{24}Mg using the symmetric-top formula of Eq. (6). Figure 7 [30, 31] shows the best correlation of theoretical levels with experiment. The 12 possible normal vibrations allowed by the structure are given in Table V. Again, the lower limits assigned to some of the rotational parameters cause the pertinent excited states to lie above 10 MeV. An excitation of a normal vibration may cause the rotor to become highly asymmetric, making the band structure of the states between 7 and 10 MeV less apparent than in ^{20}Ne. The only observed state below 9 MeV that is uncorrelated with theory is an $L^{\pi} = 3^-$ level at 7.62 MeV.

From Eqs. (14), (15), and (28), one can relate the intrinsic electric quadrupole moments to certain observed quantities. The pertinent relations are

$$\sqrt{2}\, Q_{22} \sin 2\gamma - Q_{20} \cos 2\gamma = \tfrac{2}{5}\sqrt{14\pi}\langle 2^+ \| E(2) \| 2^+ \rangle = -87 \pm 12 \text{ fm}^2,$$

$$\sqrt{2}\, Q_{22} \sin\gamma + Q_{20} \cos\gamma = 2\sqrt{\tfrac{4}{5}\pi}\langle 0^+ \| E(2) \| 2^+ \rangle = \pm 78 \pm 9 \text{ fm}^2,$$

$$\sqrt{2}\, Q_{22} \cos 2\gamma + Q_{20} \sin 2\gamma = \tfrac{2}{5}\sqrt{14\pi}\langle 2^+ \| E(2) \| 2'^+ \rangle = \pm 19 \pm 3 \text{ fm}^2,$$

$$\sqrt{2}\, Q_{22} \cos\gamma - Q_{20} \sin\gamma = 2\sqrt{\tfrac{4}{5}\pi}\langle 0^+ \| E(2) \| 2'^+ \rangle = \pm 15 \pm 3 \text{ fm}^2,$$

and

$$\sqrt{2}\, Q_{22} \cos\gamma - Q_{20} \sin\gamma = \tfrac{4}{5}\sqrt{2\pi}\langle 3^+ \| E(2) \| 2^+ \rangle = \pm 23^{+16}_{-6} \text{ fm}^2, \quad (30)$$

where the experimental values are taken from Table II and Ref. 32. A careful examination of these equations together with $|\gamma| \leq 10°$ shows that

$$Q_{20} = +75 \pm 10 \text{ fm}^2,$$

and

$$|Q_{22}| \leq 15 \text{ fm}^2. \quad (31)$$

With $\gamma = 0°$, the electron scattering form factors for ^{24}Mg are found from Eqs. (10), (11), and Fig. 5(c). These equations are

$$F^+_{00} = \tfrac{1}{3} F_\alpha [j_0(qR_1) + 2j_0(qR_2)],$$

$$F^+_{20} = \tfrac{1}{6}\sqrt{5}\, F_\alpha [-j_2(qR_1) + 4P_2(\cos\theta) j_2(qR_2)],$$

$$F^+_{40} = F_\alpha [\tfrac{3}{8} j_4(qR_1) + 2P_4(\cos\theta) j_4(qR_2)],$$

$$F^+_{22} = \tfrac{1}{6}\sqrt{15}\, F_\alpha [j_2(qR_1) - 2\sin^2\theta\, j_2(qR_2)],$$

$$F^+_{32} = 0,$$

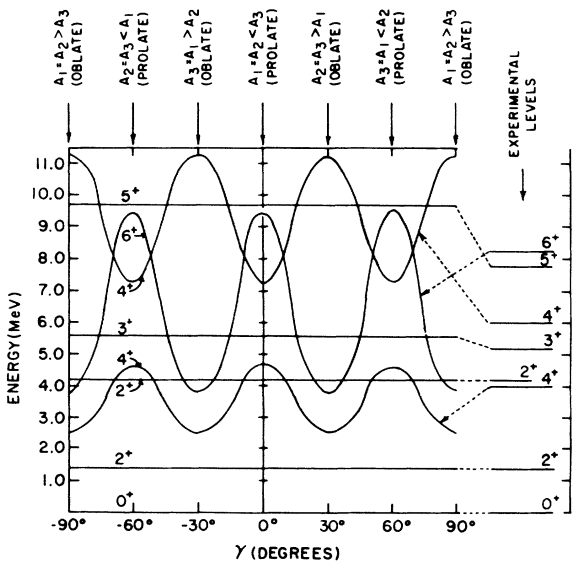

FIG. 6. Variation of theoretical energy levels of the asymmetric rotor as a function of the asymmetry parameter γ. Note that good agreement with the experimental spectrum is obtained only for $\gamma \approx 0, \pm 60°$. Inclusion of centripetal distortion would lower theoretical levels of high spin, and would give even better agreement with experiment.

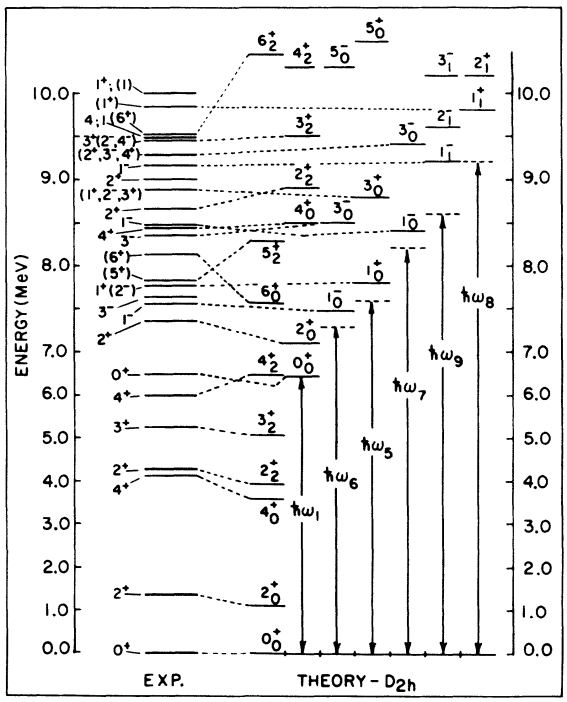

FIG. 7. Comparison of experimental levels of ^{24}Mg with the theoretical levels predicted from the D_{2h} bitetrahedron. The energy scale is again changed at 7 MeV. Experimental levels are taken from Refs. 30 and 31. The bitetrahedron can also be viewed as a D_{2h} rectangular bipyramid with the rectangle in the plane of the paper.

TABLE V. Possible normal vibrations for the D_{2h} bitetrahedron structure of ^{24}Mg.

Frequency		ω_1	ω_2	ω_3	ω_4	ω_5	ω_6	ω_7	ω_8	ω_9	ω_{10}	ω_{11}	ω_{12}
Irreducible representation	A_g	A_g	A_g	A_g	A_u	B_{1g}	B_{1u}	B_{1u}	B_{2g}	B_{2u}	B_{2u}	B_{3g}	B_{3u}
Observed energy of excitation (MeV)	0.0	6.5	···	···	···	7.6	7.3	8.2	≈9.2	≈8.6	···	···	···
Rotational parameters (MeV)													
$A_1 = A_2$	0.18	0.10	···	···	···	0.10	0.10	0.10	≈0.10	≈0.10	···	···	···
A_3	0.90	0.55	···	···	···	≥0.55	≥0.63	≥0.40	≈0.50	≈0.50	···	···	···

and

$$F_{42}^{+} = -\tfrac{1}{4}\sqrt{5}F_{\alpha}[j_4(qR_1) + 2\sin^2\theta(7\cos^2\theta - 1)j_4(qR_2)], \tag{32}$$

where R_1, R_2, and θ are defined in Fig. 5(c).

We first vary R_1, R_2, and a to agree with the elastic scattering data. The best fit is $R_1 = 1.7$ fm, $R_2 = 2.7$ fm, and $a = 1.9$ fm as shown in Fig. 8(a). These parameters are identical to the previous D_{4h} ones[14] since the two structures have the same theoretical elastic form factor. Other sets of parameters were also found which gave nearly as good results. We now vary θ to fit the inelastic curve for the 2^+ state at 1.37 MeV. The best value is $\theta = 30°$ which yields the solid line in Fig. 8(b). Theoretical curves for the cross sections of the two higher states [solid lines in Figs. 8(c) and 8(d)] are not entirely reproduced by this set of parameters. Unfortunately, the 4^+ (4.12 MeV) and 2^+ (4.23 MeV) states appear as an experimental unresolved doublet, so the theoretical cross sections of these two levels must be added. As expected, scattering to the 3^+ state at 5.22 MeV was not experimentally observed.

The results can be improved somewhat if we also vary the asymmetry parameter γ. Since we now have an asymmetric rotor, the cross sections cannot be found in simple forms, but are still com-

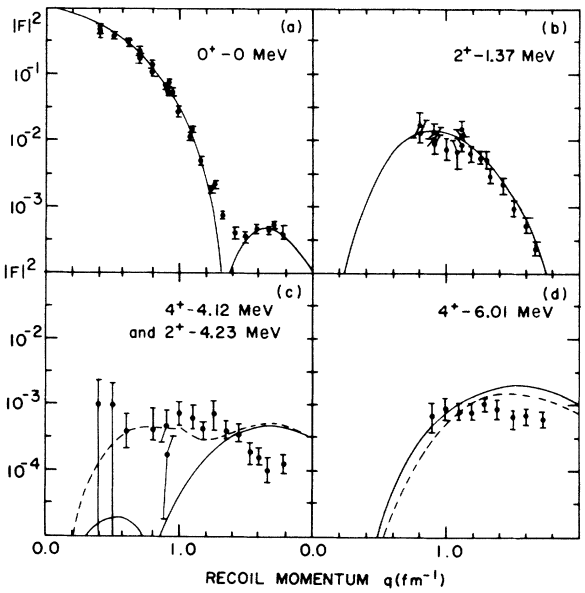

FIG. 8. Experimental and theoretical form factors for the D_{2h} bitetrahedron of ^{24}Mg: (a) elastic scattering form factor; (b)–(d) various inelastic scattering form factors. Centripetal distortion, which has the effect of compressing the theoretical curves towards the ordinate axis (as shown in Figs. 4 and 11), was not considered because of the number of parameters already used. Inclusion of this effect would definitely give better results for Figs. 8(c) and 8(d).

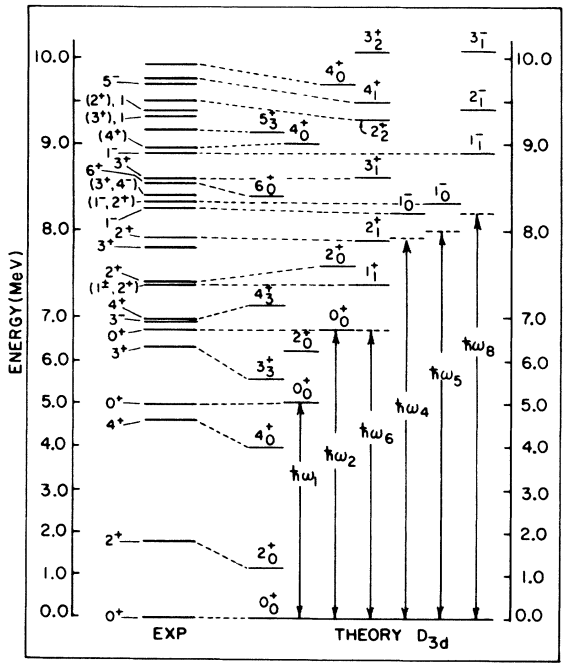

FIG. 9. Comparison of the experimental levels of ^{28}Si with the theoretical levels predicted from the oblate D_{3d} structure. The energy scale is again changed at 7 MeV, and experimental levels are taken from Refs. 30 and 33.

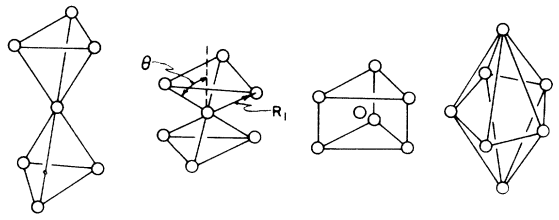

FIG. 10. (a)–(d) Some of the possible configurations for ^{28}Si.

puted from Eqs. (10) and (11). Here is where we make use of the fact that the a^L_{NK} depend upon only one parameter, which in this case is γ. Like θ, this parameter has no effect on the elastic scattering cross section of Fig. 8(a). The dashed lines in Figs. 8(c) and 8(d) represent the same parameters as before, except that the asymmetry parameter is now $\gamma = +10°$. The form factor for the 2^+ (1.37 MeV) level is only slightly altered by this change in γ and is not shown in Fig. 8(b). Since R_1, R_2, θ, and γ have now been determined, we can calculate the intrinsic quadrupole moments, which are $Q_{20} = 61.2$ fm^2 and $Q_{22} = -3.7$ fm^2, close to the values given in Eq. 31. Reasonable values of the five parameters (R_1, R_2, a, θ, and γ) have thus led to four good cross-section curves. In addition, these same parameters correctly predict several reduced matrix elements.

^{28}Si

Looking at the experimental spectrum of ^{28}Si (Fig. 9 [30, 33]). We find that the lowest three levels indicate some form of collective rotation. However, these levels do not follow the $L(L+1)$ rule as well as the corresponding levels in ^{20}Ne and ^{24}Mg. There also appear to be $K^\pi = 3^+$ and $K^\pi = 3^-$ bands starting at 6.27 and 6.88 MeV, respectively. The D_{3d} bitetrahedron [(Fig. 10(a)], which was considered to be the best structure in a previous paper,[15] can account for both bands if one allows for the possibility of internal rotation between the two triangular clusters. The calculations are very similar to those already done for the D_{2d} hindered rotor in ^{20}Ne, the small energy separation between the two $K = 3$ bands implying that this structure has nearly free internal rotation. Unfortunately, recent experiments that measure the static quadrupole moment of the 2^+ (1.78 MeV) state show that ^{28}Si is oblate, a fact definitely eliminating Fig. 10(a) as a possible structure. An oblate D_{3d} structure as shown in Fig. 10(b) leads to only the $K = 3^+$ band. Similarly, the oblate D_{3h} structure of Fig. 10(c) predicts only the $K^\pi = 3^-$ band. The D_{5h} bipyramid [Fig. 10(d)], which is the usual configuration considered for ^{28}Si, predicts only $K^\pi = 1^\pm$, $2^\pm$, or 5^- bands in this region (c.f., Table I). A planar D_{6h} hexagon with one α cluster in the center can account for both $K = 3$ bands by assuming they are built on separate normal vibrations. However, this structure is unlikely; it leads to a negative intrinsic quadrupole moment twice as large as experiment. Other configurations besides those already mentioned were considered in Ref. 15 and discarded.

Of the configurations that have the proper quadrupole moment, the one that predicts the most low-lying energy levels is the oblate D_{3d} structure of Fig. 10(b). The K^π bands allowed for each IR of D_{3d} are given in Table I, and the possible normal vibrations are listed in Table VI along with values for the excitation energies of observed normal vibrations. Again, in order to push certain states above 10 MeV, lower limits are given to several of the rotational parameters. The results are not as good as for the previous two nuclei. A low-lying $L^\pi = 2^+$ state is predicted at approximately 6.2 MeV which is not observed (Fig. 9). However, this state would also be predicted by all other symmetric-top configurations. As in ^{24}Mg, the lowest state observed but not predicted is a 3^- state at 6.88 MeV.

TABLE VI. Possible normal vibrations for the oblate D_{3d} structure of ^{28}Si.

Frequency	•••	ω_1	ω_2	ω_3	ω_4	ω_5	ω_6	ω_7	ω_8	ω_9	ω_{10}
Irreducible representation	A_{1g}	A_{1g}	A_{1g}	A_{1u}	A_{2u}	A_{2u}	E_g	E_g	E_u	E_u	E_u
Observed energy of excitation (MeV)	0	5.0	6.7	•••	≈7.9	≈8.0	6.7	•••	≈8.2	•••	•••
Rotational parameters (MeV)											
$A_1 = A_2$	0.20	0.20	0.15	•••	≳0.18	≥0.17	0.12	•••	0.12	•••	•••
A_3	0.55	≥0.49	≥0.32	•••	•••	•••	0.60	•••	≈0.6	•••	•••

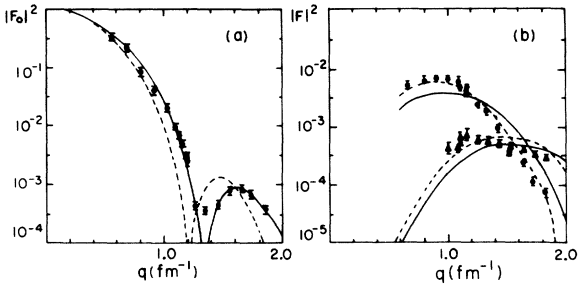

FIG. 11. Experimental and theoretical form factors for ^{28}Si: (a) elastic scattering form factors, (b) inelastic scattering form factors for the 1.78-MeV 2^+ state (●), and the 4.61-MeV 4^+ state (▲).

The theoretical form factors for the low-lying $K^\pi = 0^+$ states of this structure are:

$$F_{00}^{+} = \tfrac{1}{7}F_\alpha[1 + 6j_0(qR_1)],$$
$$F_{20}^{+} = \tfrac{6}{7}\sqrt{5}F_\alpha P_2(\cos\theta)j_2(qR_1),$$
$$F_{40}^{+} = \tfrac{18}{7}F_\alpha P_4(\cos\theta)j_4(qR_2). \quad (33)$$

Comparing these equations with experiments taken from Ref. 14, one finds that the elastic scattering form factor can only be well predicted if one assumes that the central α particle is slightly larger than the other six. In this case, only the elastic form factor changes, becoming

$$F_{00}^{+} = \tfrac{1}{7}[e^{-q^2a_0^2/6} + 6j_0(qR_1)e^{-q^2a^2/6}]. \quad (34)$$

Since these formulas are independent of the azimuthal angle of the α clusters, they also apply to the oblate D_{3h} structure of Fig. 10(c).

The experimental elastic scattering curve can now be reproduced very well with several different sets of parameters [Fig. 11(a)]. However, all of them predict the parameter a_0 to be about 0.2 fm larger than a. The angle θ can then be varied to fit the 2^+ (1.78 MeV) curve. The solid line in Fig. 11 represents the best fit with $a_0 = 1.9$ fm, $a = 1.7$ fm, $R_1 = 2.65$ fm, and $\theta = 63°$. The theoretical form factor for the 2^+ state can be improved if one allows for centripetal distortion by increasing R_1. This improvement is shown in Fig. 11(b) by the dashed curve which is drawn for $a_0 = 1.9$ fm, $a = 1.7$ fm, $R_1 = 3.0$ fm, and $\theta = 64°$. Naturally, one expects these new parameters to give a poorer fit for the elastic curve. Using $R_1 = 3.0$ fm and $\theta = 64°$, the intrinsic quadrupole moment is found to be $Q_{20} = -45.8$ fm^2 which compares favorably with the value obtained from the measured 2^+ static quadrupole moment of Table II, as well as with the moment determined from various transitions (Table VII).

A similar calculation[14] of the form factors has been done for ^{28}Si with the D_{5h} pentagonal bipyramid of Fig. 10(d). As in the D_{3d} case, new values for the parameters were needed to fit the inelastic scattering curves. Although the resultant theoretical curves are equally as good as those given in Fig. 11, the parameters for inelastic scattering needed to be changed in the opposite direction from that which one would expect for centripetal distortion. Since the D_{3d} structure also predicts most of the observed low-lying levels, it should be preferred over the D_{5h} bipyramid.

^{32}S and ^{36}Ar

It is interesting to note that the energy spectra of both ^{32}S and ^{36}Ar (Figs. 12 and 13) have 0^+, 2^+, 4^+, and 3^- levels at approximately twice the energy of the first 2^+ state in good agreement with the collective vibrator model. Moreover, no definite K^π bands other than possibly the ground-state 0^+ band are observed in either nuclei. Also, from the last column of Table II, it appears that the low-lying states of ^{32}S are not of the same character as those of ^{20}Ne, ^{24}Mg, and ^{28}Si. As a consequence, one does not expect the CAP model to work as well here as for the nuclei previously considered.

Most of the possible structures for ^{32}S appear in Ref. 15, where it was concluded that this nucleus most likely had D_{3d} or D_{3h} symmetry. Reviewing

TABLE VII. Comparison of theoretical and experimental values for certain transitions in ^{28}Si using the D_{3d} structure. The single parameter is taken to be $|Q_{20}| = 50.2$ fm^2.

Initial-state energy L^π (MeV)	Final-state energy L^π (MeV)	Type of transition	Transition rate $\|M^2\|$ (in Weisskopf units) Experiment	Theory
2^+ 1.78	0^+ 0.0	$E2$	14.7 ± 1.6 [a]	10.0
4^+ 4.61	2^+ 1.78	$E2$	9.5 ± 2.2 [a]	14.3
6^+ 8.54	4^+ 4.61	$E2$	9.4 ± 3.0 [a]	15.7
3^+ 6.27	2^+ 1.78	$E2$	0.001 [b]	0.0
4^+ 6.89	2^+ 1.78	$E2$	1.1 ± 0.2 [b]	0.0
3^- 6.88	0^+ 0.0	$E3$	18.0 ± 13.0 [b]	...

[a] Reference 33.
[b] M. M. Aleonard, D. Castera, P. Hubert, F. Leccia, P. Mennrath, and J. P. Thibaud, Nucl. Phys. A146 90 (1970).

the calculations with more recent and extensive experimental data, we find that D_{3h} and D_{2h} structures (Fig. 14) give reasonable fits, with a D_{3d} structure not completely ruled out. Results for the D_{2h} and D_{3h} structures are plotted in Fig. 12, together with the experimental data.[30, 34] Unlike our calculations for the previous nuclei, the same set of rotational parameters is used over all normal vibrations. Again, for both structures, the first level observed but not predicted is of spin $L = 3$ at around 5 MeV. Structures of higher symmetry [such as the D_{6h} hexagonal bipyramid, Fig. 14(b), the D_{7h} body-centered planar heptagon, etc.] can account for all low-lying levels if one introduces five or six normal vibrations. However, these structures predict an oblate shape contrary to experiment, and introduce too many parameters to be really meaningful.

The nucleus ^{36}Ar is similar to ^{20}Ne and ^{28}Si in that it contains an odd number of α clusters. Since both ^{20}Ne and ^{28}Si were found to have an α particle in the center, one of the most likely candidates for ^{36}Ar is the D_{4d} body-centered square antiprism of Fig. 14(c). Another possibility is the D_{5h} planar pentagon, where four of the α clusters form an ^{16}O core [Fig. 14(d)]. Both of these structures give fair agreement with experiment[30] as is shown in Fig. 13. The first level observed but not predicted is an $L = 3^-$ level at 4.18 MeV. Again, configurations of higher symmetry can account for all levels if enough parameters are introduced, but such agreement is not very satisfying.

It should be noted that both structures given for ^{36}Ar have double vibrations [denoted $\hbar\omega_3$ in Figs. 13(a) and 13(b)] which occur at relatively low energy. Unlike the corresponding ω_8 double vibration of ^{20}Ne, both of these modes contain two quanta of a doubly degenerate vibration. The allowed IR's for these modes are thus found by taking the appropriate symmetric direct product.[35] All antisymmetric wave functions of the direct product will identically vanish.

^{40}Ca

Unlike all other nuclei considered in this paper, ^{40}Ca does not have $L^\pi = 2^+$ for its first excited state [c.f., Fig. 15(a)]. Consequently, ^{40}Ca has no permanent quadrupole deformation in its ground state and the momental ellipsoid of any α structure for this nucleus must be that of a spherical top (i.e., $A_1 = A_2 = A_3$). The only reasonable configuration satisfying these conditions is the structure

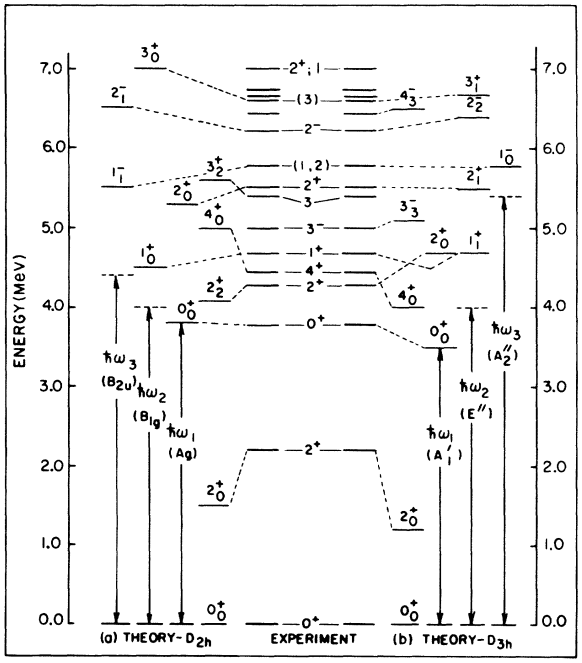

FIG. 12. Comparison of experimental levels of ^{32}S with theory predicted from two different structures. Also shown are the IR's for the observed normal modes. The parameters used (in MeV) are: (a) D_{2h} structure: $A_1 = A_2 = 0.25$, $A_3 = 0.90$, $\hbar\omega_1 = 3.8$, $\hbar\omega_2 = 4.0$, and $\hbar\omega_3 = 4.4$; (b) D_{3h} structure: $A_1 = A_2 = 0.20$, $A_3 = 0.50$, $\hbar\omega_1 = 3.5$, $\hbar\omega_2 = 4.0$, and $\hbar\omega_3 = 5.4$.

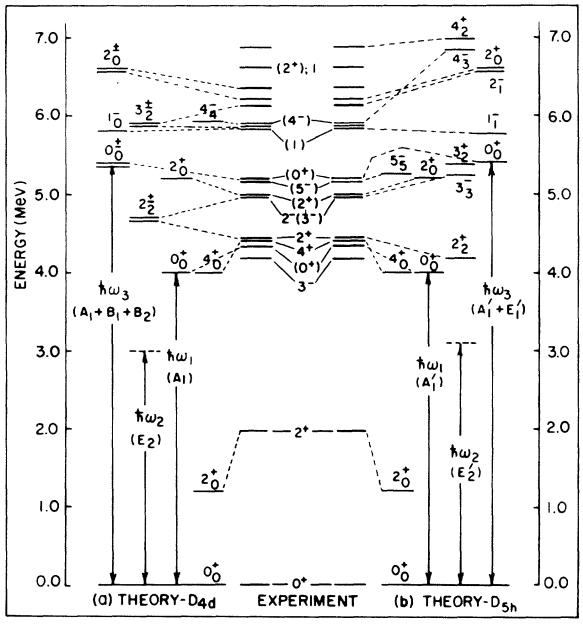

FIG. 13. Comparison of experimental levels of ^{36}Ar with theory predicted by two different structures. The IR's for observed normal modes are also shown. In both structures, the vibration that contains two quanta of $\hbar\omega_2$ occurs at relatively low energy and is denoted $\hbar\omega_3$. The parameters used (in MeV) are: (a) D_{4d} structure: $A_1 = A_2 = 0.20$, $A_3 = 0.32$, $\hbar\omega_1 = 4.0$, $\hbar\omega_2 = 3.0$, and $\hbar\omega_3 = 5.4 \lesssim 2\hbar\omega_2$. (b) D_{5d} structure: $A_1 = A_2 = 0.20$, $A_3 = 0.17$, $\hbar\omega_1 = 4.0$, $\hbar\omega_2 = 3.1$, and $\hbar\omega_3 = 5.4 \lesssim 2\hbar\omega_2$.

shown in Fig. 15(b). It consists of six α clusters arranged in an octahedron outside of four others which form a tetrahedral ^{16}O core. The similarity of this structure with the corresponding shell-model description is especially appealing.

The low-lying excited states of this structure should be very complicated because one now has 10 particles to contend with, and also because Coriolis forces are known to be extremely important in spherical-top configurations.[6] Indeed, there is even reason to believe that some of the excited states, such as the first excited 0^+, 2^+, and 4^+ levels, may be built on permanently deformed rotational bands. A similar situation is known to exist in ^{16}O.[26] As a first approximation, one could assume that the ^{16}O core does not contribute to the over-all rotation of the nucleus. The structure would then have 0_h symmetry, and the first three negative-parity states could be qualitatively explained as rotational states built on a normal vibration of the F_{1u} IR, which contains levels of spin $L^\pi = 3^-$, 4^-, 5^-, $6^-, \ldots$.[35] Because of the complexity of the problem, no attempt was made to calculate the level spectrum explicitly.

From recent experiments,[36,37] the absolute form factor ($|F_{00}^+|$) for elastic electron scattering on ^{40}Ca is known very well, and is shown as the dotted curve in Fig. 15(c). This curve was obtained indirectly in Refs. 36 and 37 by first fitting a phenomological charge distribution of six parameters to experimental differential cross sections, using partial-wave analysis, and then calculating $|F_{00}^+|$ by taking the Fourier transform of this charge distribution. Because of the method used, no error bars were drawn for this curve, but they should be quite small except for possibly $q \geq 3$ fm^{-1}. All present experiments give points between 0.7 fm^{-1} $\leq q \leq 3.2$ fm^{-1}.

The theoretical form factor factor is obtained directly from Eqs. (10), (11), and Fig. 15(b) as

$$|F_{00}^+| = \tfrac{1}{10} e^{-q^2a^2/6}[4j_0(qR_1) + 6j_0(qR_2)], \qquad (35)$$

where R_1 and R_2 are the radial distances to the α clusters in the tetrahedron and octahedron, respectively. The best over-all fit is with $a = 1.7$ fm, $R_1 = 2.2$ fm, and $R_2 = 3.9$ fm. If one changes R_1 and R_2 to 2.1 and 3.6 fm, the first two maxima are better reproduced, but the fit above 2.0 fm^{-1} is destroyed. The agreement between theory and experiment is also improved if one introduces a fourth parameter by allowing the rms radii of the inner and outer α clusters to differ. It is interesting to note that the second minimum of the theoretical curve does not go to 0. This fact leads to some interesting results that will be examined more closely in the next section.

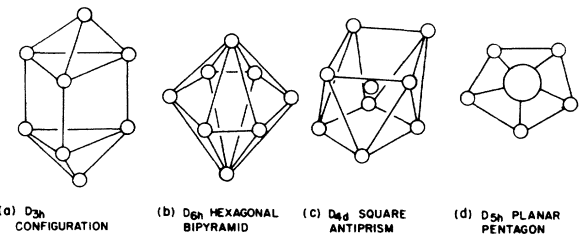

FIG. 14. Two possible configurations each for ^{32}S [Figs. (a) and (b)], and ^{36}Ar [Figs. (c) and (d)].

IV. MASS SHAPES AND CHARGE DISTRIBUTIONS

As a result of the calculations in the preceding section, the CAP model can now predict the position and rms radius of each internal α cluster for all nuclei listed in the first column of Table VIII. Thus it is possible to calculate classically the "rigid" moments of inertia for these nuclei and compare them to the "effective" moments that are needed to reproduce their energy spectra. Table VIII compares the "effective" and "rigid" rotational parameters which vary as the reciprocal of the moments. From this table, one sees that the "rigid" moments are usually twice as large as the "effective" moments for rotations about the x or y axis, and three to four times as large for rotations about the symmetry axis. This is not unex-

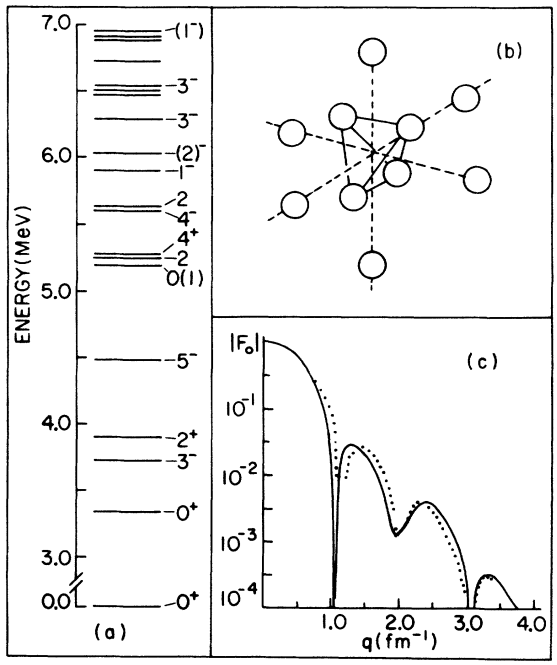

FIG. 15. (a) Energy levels of ^{40}Ca (in MeV). (b) The most realistic α structure for ^{40}Ca is an octahedron outside of a tetrahedral ^{16}O core. (c) Comparison of experimental elastic electron form factor with that predicted by the structure in (b).

pected since a similar situation occurs for deformed nuclei in the regions $150 < A < 190$ and $A > 220$.

Finally, we calculate the effective radial charge distribution for several different nuclei by averaging the charge distribution of Eq. (8) over all possible orientations. This is accomplished by taking the inverse Fourier transform of the elastic scattering form factor. From Eqs. (10) and (11), we find

$$F_{00}^{+} = \frac{e^{-q^2a^2/6}}{n} \sum_{i=1}^{n} j_0(qR_i), \tag{36}$$

and a straightforward integration yields

$$\rho(r) = \frac{2e}{ar}\left(\frac{3}{8\pi^3}\right)^{1/2} \sum_{i=1}^{n} \frac{1}{R_i} e^{-3(r^2+R_i^2)/2a^2} \sinh\frac{3R_i r}{a^2}, \tag{37}$$

where $\rho(r)$ is the radial charge distribution of the nucleus normalized to the proton charge, $2ne$.

Figure 16(a), taken from Ref. 8, shows the radial charge distributions for α-particle configurations of ^{12}C and ^{16}O. The D_{5h} curve in Fig. 16(c) is computed from parameters given in Ref. 14; this distribution also fits the experimental $|F_{00}^{+}|^2$ for ^{28}Si [given in Fig. 11(a)]. The phenomenological fit to ^{40}Ca in Fig. 16(d) is taken from Ref. 37. All other curves are calculated from parameters given in the present paper. The two charge distributions for ^{28}Si have essentially the same absolute elastic form factor up to 1.8 fm^{-1}, but they can be shown to vary considerably above this value. In particular, the third maximum of $|F_{00}^{+}|^2$ for the D_{3d} structure is calculated to be 100 times as large as that of the D_{5h} case. Future experiments on the elastic scattering form factors of ^{28}Si at higher energies will thus favor one distribution over the other. On the other hand, the absolute form-factor curve for ^{40}Ca is known well up to 3.2 fm^{-1}, and both distributions of Fig. 16(d) give approximately the same $|F_{00}^{+}|$ through the fourth maximum. The large difference in the two distributions is thus probably due to the fact that the phenomenological fit assumes the form factor changes sign at the second minimum (as shown in Ref. 36), whereas the form factor for the α structure does not [c.f., Fig. 15(c)]. Although the absolute values of the form factors of the two distributions are nearly the same, the actual form factors are quite different above 2.0 fm^{-1}. In fact, by slightly altering the present charge distribution,

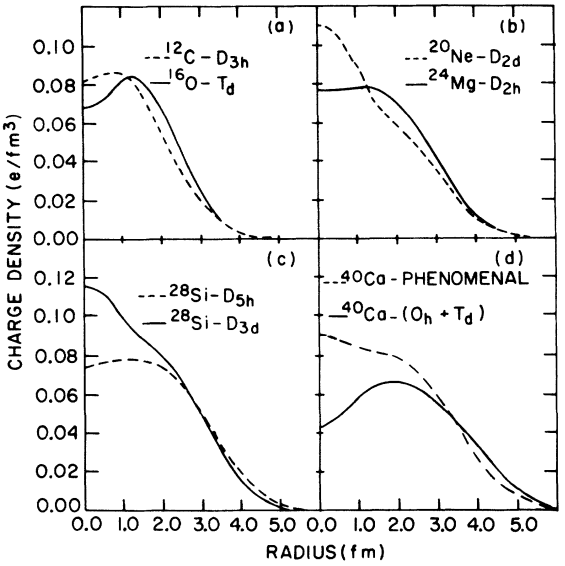

FIG. 16. (a)–(d) Radial charge distributions of various light $A = 4N$ nuclei predicted by the CAP model. The assumed structure of each nucleus is also given.

TABLE VIII. Comparison of "rigid" and "effective" rotational parameters for several light nuclei. The spatial parameters needed to calculate the "rigid" A_j's were found by applying the CAP model to electron scattering data. Information needed for $1p$-shell nuclei was obtained from previous papers (Ref. 8). In order to make the calculations more realistic, the center α clusters of ^{20}Ne and ^{28}Si were assumed not to contribute to the "rigid" moments of inertia.

	Assumed α structure	Levels used in calculating "effective" rotational parameters (MeV)	Calculated rotational parameters (MeV) "Effective" $A_1=A_2$	"Effective" A_3	"Rigid" $A_1=A_2$	"Rigid" A_3
^{9}Be	$D_{\infty h}$ dumbbell with neutron	$\frac{5}{2}^-$, 2.43	0.48		0.51	
^{12}C	D_{3h} equilateral triangle	2^+, 4.43 3^-, 9.64	0.74	0.82	0.51	0.35
^{16}O	T_d tetrahedron	3^-, 6.13	0.51	0.51	0.28	0.28
^{20}Ne	D_{2d} distorted tetrahedron	2^+, 1.63 2^-, 4.97	0.27	1.10	0.14	0.32
^{24}Mg	D_{2h} bitetrahedron	2^+, 1.37 2^+, 4.23	0.23	0.94	0.12	0.19
^{28}Si	Oblate D_{3d} structure	2^+, 1.78 3^+, 6.27	0.30	0.60	0.12	0.14

which is somewhat hollow in the center, one should be able to calculate differential cross-section curves just as good as those obtained for the previous phenomenological distribution. Since the Born approximation can no longer be used for such an exact calculation, no attempt is made at present to validate this assumption.

V. COMPARISON WITH OTHER MODELS AND CONCLUSIONS

From the preceding discussion, it appears that the model works very well at the beginning of the $2s$-$1d$ shell, but has only moderate success for nuclei above ^{24}Mg. All observed K^π bands of ^{20}Ne under 9 MeV can be predicted with the D_{2d} distorted tetrahedron, while ^{24}Mg is well described by a D_{2h} bitetrahedron. The results for ^{28}Si are not as conclusive as for the previous two nuclei, though present data favor an oblate D_{3d} structure over the more familiar D_{5h} pentagonal bipyramid. The structures assumed for ^{24}Mg and ^{28}Si both give good agreement with the experimental electron scattering form factors. Several structures do a fair job in predicting the energy levels of ^{32}S and ^{36}Ar. However, in both of these nuclei, low-lying levels are observed that are not well predicted. The nucleus ^{40}Ca is found to have an α structure of 0_h symmetry. Although the energy spectrum is only qualitatively discussed, the experimental elastic form factor for electron scattering is well described. The first energy level observed but not predicted is usually a 3^- state. These levels may have a large contribution from an octopole vibration which is not part of the CAP model.

In recent years deformed Hartree-Fock (DHF),[38,39] SU_3,[40,41] intermediate-coupling,[42] and unified collective models[43] have all been applied to many nuclei in the $2s$-$1d$ shell. The DHF calculations usually allow the nucleus to have only axial or ellipsoidal (i.e., D_{2h} symmetry) deformations. However, even with these restricted deformations, some interesting comparisons with the CAP model can be made. The ground-state DHF structures for ^{20}Ne and ^{24}Mg are definitely prolate, but an oblate structure is found to be slightly favored in ^{28}Si. These results are in good agreement with experiment (c.f., Table II) as well as with our structures. In addition, ^{24}Mg appears to prefer an ellipsoidal rather than an axially symmetric shape; this qualitatively agrees with our D_{2h} bitetrahedron [Fig. 5(c)]. Ripka (Ref. 38) has plotted some very informative density distribution curves for his axially symmetric DHF solutions of ^{12}C, ^{20}Ne, and ^{28}Si. The irregularities in the equi-density surface show good evidence for four-body correlations in all three nuclei. For example, ^{12}C is shown to be oblate and hollow in the center (i.e., toroidal shaped), which is in close agreement with the triangular α structure assumed by the CAP model. The density plot of ^{20}Ne seems to differ from our results as it favors the D_{3h} bipyramid [Fig. 1(c)] over the D_{2d} distorted tetrahedron [Fig. 1(a)]. One possible explanation for this discrepancy is that D_{2d} distortions were not allowed in the DHF calculations. Unfortunately no density plot was given for ^{24}Mg.

The present paper shows how the CAP model gives an especially simple explanation for the opposite parities of the $K = 2$ bands in ^{20}Ne and ^{24}Mg. As noted before, other collective models, especially the asymmetric rotor, can account for the $K^\pi = 2^+$ band in ^{24}Mg, but the negative-parity bands in ^{20}Ne are usually explained by promoting the $1p$-shell nucleon to the $2s$-$1d$ shell. In the unified Nilsson model, this promotion results in several different bands,[43] and it is difficult to tell which ones are lowest in energy. This difficulty is removed in the SU_3 model because one assumes that the lowest states are those of maximum orbital symmetry. Thus the negative-parity states of ^{20}Ne are presumed to be built on the $(\lambda\mu) = (82)$ or (90) irreducible representation of SU_3; the former is a five-particle–one-hole state, while the latter is obtained on promoting a $2s$-$1d$-shell nucleon to the next higher shell. Using Elliott's projection scheme, one finds that the (82) space yields $K^\pi = 2^-$ and $K^\pi = 0^-$(L even) bands, while the (90) space has only a $K^\pi = 0^-$ (L odd) band. The first and third bands are observed experimentally (Fig. 2), but they are also explained by the CAP in a quite different manner. The SU_3 model can also explain the $K^\pi = 0^+$ and $K^\pi = 2^+$ bands of ^{24}Mg as belonging to the $(\lambda\mu) = (84)$ irreducible representation. Harvey (Ref. 40) has plotted the particle probability density distribution for the intrinsic part of this particular state; the contour lines again show correlation and seem to favor the D_{2h} bitetrahedron of Fig. 5(c).

Finally, we compare our α structures with those of Brink and co-workers[26] who have recently applied HF calculations to many-particle α-cluster wave functions for all $4N$ nuclei between ^{12}C and ^{28}Si. They find the most stable configurations to be the D_{3h} trigonal bipyramid for ^{20}Ne, the D_{4h} square bipyramid for ^{24}Mg, and a prolate D_{3h} structure for ^{28}Si; the first two are shown in Figs. 1(c) and 5(a), respectively. None of these structures is in agreement with the results of the present paper; however, it is not known if our structures for ^{20}Ne and ^{24}Mg were actually considered in their calculations. A number of authors have also searched for α correlations by relaxing the restrictions of the DHF calculations.[44,45] Instead

of axial or ellipsoidal deformations, they allow for deformations of less symmetry which do not inhibit cluster formations. One of these papers[45] imposed trigonal symmetries on ^{12}C, ^{16}O, and ^{20}Ne, and found α correlations in all three nuclei when a Volkov force was used with a sufficiently strong Majorana exchange term ($M = 0.75$). So far as we are aware, no DHF calculation has been performed on ^{20}Ne with D_{2d} symmetry.

The results of this paper also give a qualitative estimate of the stability of these internal α clusters. If the clusters were long-lived compared with their relative motions, one would expect the short-range interactions between these clusters to favor those structures having the greatest number of bonds. The present work shows that this is not always the case, since nonbipyramid shapes were found for ^{20}Ne, ^{24}Mg, and ^{28}Si. This result implies that the clusters may be quite transient but still permanent enough to impress some over-all point group symmetry on the single-particle shell-model states. One would expect that the symmetry relations of the CAP model still hold for this more realistic situation. Indeed, Herzenberg[46] and Brink[5] have each shown that these symmetry conditions still apply for two different types of microscopic cluster models. In fact, the frequent interchange of nucleons between α clusters should make them more cohesive and add to the total rigidity of the α structure.

In summary the phenomenological CAP model seems to give a good basic description of the low-lying levels of several light $4N$ nuclei, and it also indicates which symmetries are important for each nucleus. These symmetries should in turn dictate how one can best proceed with more realistic calculations.

---

*Work performed in part in the Ames Laboratory of the U. S. Atomic Energy Commission. Contribution No. 2954.

[1]D. M. Brink, in *Many-Body Description of Nuclear Structure and Reactions, Proceedings of the International School of Physics, "Enrico Fermi," Course XXXVI, 1966,* edited by C. Bloch (Academic Press Inc., New York, 1967), p. 247.

[2]J. A. Wheeler, Phys. Rev. 52, 1083 (1937); W. Wefelmeir, Naturwiss. 25, 525 (1937).

[3]A. Herzenberg, Nuovo Cimento 1, 986, 1008 (1955); Nucl. Phys. 3, 1 (1957); A. Herzenberg and A. S. Roberts, *ibid.* 3, 314 (1957).

[4]J. K. Perring and T. H. R. Skyrme, Proc. Phys. Soc. (London) A69, 600 (1956); J. V. Noble, Phys. Letters 31B, 253 (1970); Phys. Rev. C 1, 1900 (1970).

[5]D. M. Brink and A. Weiguny, Nucl. Phys. A120, 59 (1968).

[6]D. M. Dennison, Phys. Rev. 96, 378 (1954); S. L. Kameny, *ibid.* 103, 358 (1956).

[7]A. E. Glassgold and A. Galonsky, Phys. Rev. 103, 701 (1956).

[8]E. V. Inopin and B. I. Tishchenko, Zh. Eksperim. i Teor. Fiz. 38, 1160 (1960) [transl.: Soviet Phys.–JETP 11, 840 (1960)]; V. Vadia, E. Inopin, and M. Yosev, Zh. Eksperim. i Teor. Fiz. 45, 1164 (1963) [transl.: Soviet Phys.–JETP 18, 802 (1964)].

[9]L. C. McDonald and H. Überall, Phys. Rev. C 1, 2156 (1970).

[10]A. I. Baz', Zh. Eksperim. i Teor. Fiz. 31, 831 (1956) [transl.: Soviet Phys.–JETP 4, 704 (1957)].

[11]S. Matthies, V. G. Neudachin, and Yu. F. Smirnov, Zh. Eksperim. i Teor. Fiz. 42, 592 (1962) [transl.: Soviet Phys.–JETP 15, 411 (1962)]; Nucl. Phys. 38, 63 (1962).

[12]P. Goldhammer, Rev. Mod. Phys. 35, 40 (1963).

[13]E. V. Inopin, A. A. Kresnin, and B. I. Tishchenko, Yadern. Fiz. 2, 802 (1965) [transl.: Soviet J. Nucl. Phys. 2, 573 (1966)].

[14]G. A. Savitskii, N. G. Afanas'ev, I. S. Gul'karov, V. M. Khvastunov, A. A. Khomich, and N. G. Shevchenko, Yadern. Fiz. 7, 1181 (1968) [transl.: Soviet J. Nucl. Phys. 7, 705 (1968)].

[15]D. L. Nordstrom, J. A. Tunheim, and G. H. Duffey, Phys. Rev. 145, 727 (1966).

[16]P. S. Hauge and G. H. Duffey, Phys. Rev. 152, 1023 (1966).

[17]G. Herzberg, *Infrared and Raman Spectra of Polyatomic Molecules* (D. Van Nostrand Company, Inc., New York, 1945), pp. 42–55, 82–130, 370–376, 491–500.

[18]M. Bouten, Nuovo Cimento 26, 63 (1962).

[19]E. B. Wilson, Jr., J. Chem. Phys. 3, 278 (1935).

[20]E. B. Wilson, Jr., J. C. Decius, and P. C. Cross, *Molecular Vibrations* (McGraw-Hill Book Company, Inc., New York, 1955), pp. 361–370, 92–101.

[21]B. P. Nigam and R. R. Roy, *Nuclear Physics* (John Wiley & Sons, Inc., New York, 1967), pp. 21, 271–275, 292–301.

[22]H. Frank, D. Haas, and H. Prange, Phys. Letters 19, 391 (1965); R. F. Frosch, J. S. McCarthy, R. E. Rand, and M. R. Yearian, Phys. Rev. 160, 874 (1967).

[23]K. Alder, A. Bohr, T. Huus, B. Mottleson, and A. Winther, Rev. Mod. Phys. 28, 432 (1956).

[24]We have fitted the energy levels and electron scattering form factors by visual means. In order to justify a χ^2 procedure, one would have to handle the rotation-vibration interactions in a more fundamental way. Furthermore, higher-order terms in the Born expansion would be expected to contribute somewhat to the electron scattering cross sections.

[25]E. Teller and J. A. Wheeler, Phys. Rev. 53, 778 (1938).

[26]D. M. Brink, H. Friedrich, A. Weiguny, and C. W. Wong, Phys. Letters 33B, 143 (1970).

[27]J. A. Kuehner and E. Almqvist, Can. J. Phys. 42, 489 (1964); 45, 1605 (1967).

[28]F. Ajzenberg-Selove and T. Lauritsen, Nucl. Phys. 11, 1 (1959).

[29]C. H. Townes and A. J. Schawlow, *Microwave Spectroscopy* (McGraw-Hill Book Company, Inc., New York,

1955), pp. 300–335.
[30]P. M. Endt and C. Van der Leun, Nucl. Phys. 105, 1 (1967).
[31]R. W. Ollerhead, J. A. Kuehner, R. J. A. Levesque, and E. W. Blackmore, Can. J. Phys. 46, 1381 (1968).
[32]S. W. Robinson and R. D. Bent, Phys. Rev. 168, 1266 (1968).
[33]F. C. P. Huang and D. K. McDaniels, Phys. Rev. C 2, 1342 (1970).
[34]G. T. Garvey, K. W. Jones, L. E. Carlson, A. G. Robertson, and D. F. H. Start, Phys. Letters 29B, 108 (1969).
[35]M. Hamermesh, *Group Theory* (Addison-Wesley Publishing Company, Inc., Reading, Massachusetts, 1964), pp. 132–134, 339.
[36]J. B. Bellicard *et al.*, Phys. Rev. Letters 19, 527 (1967).
[37]R. F. Frosch *et al.*, Phys. Rev. 174, 1380 (1968).
[38]G. Ripka, in *Advances in Nuclear Physics*, edited by M. Baranger and E. Vogt (Plenum Press, Inc., New York, 1968), Vol. I, pp. 183–259.
[39]J. Bar-Touv, in *Many-Body Description of Nuclear Structure and Reactions, Proceedings of the International School of Physics "Enrico Fermi," Course XXXVI, 1966*, edited by C. Bloch (Academic Press Inc., New York, 1967), pp. 453–463; J. Bar-Touv and I. Kelson, Phys. Rev. 138, B1035 (1965).
[40]M. Harvey, in *Advances in Nuclear Physics*, edited by M. Baranger and E. Vogt (Plenum Press, Inc., New York, 1968), Vol. I, pp. 67–151.
[41]G. J. Borse and J. M. Eisenberg, Phys. Letters 22, 630 (1966); J. E. Stover, Nucl. Phys. A92, 209 (1967).
[42]M. C. Boaten, J. P. Elliot, and J. A. Pullen, Nucl. Phys. A97, 113 (1967).
[43]R. H. Siemssen and L. L. Lee, Jr., Phys. Rev. 140, B1258 (1965).
[44]N. Onishi and R. K. Sheline, Nucl. Phys. A165, 180 (1971); W. Wadia, Z. Physik 224, 425 (1969).
[45]J. Eichler and A. Faessler, Nucl. Phys. A157, 166 (1970).
[46]A. Herzenberg, Nuovo Cimento 1, 1008 (1955).

PHYSICAL REVIEW C VOLUME 4, NUMBER 4 OCTOBER 1971

Total Cross Section of Protons for 2.5-MeV Neutrons

J. C. Davis,* K. A. Weaver,*† D. Hilscher,‡ and H. H. Barschall*
University of Wisconsin, Madison, Wisconsin 53706§

and

A. B. Smith
Argonne National Laboratory, Argonne, Illinois 60439§

(Received 9 July 1971)

The total cross section of protons for neutrons of mean energy 2535 keV was measured to be 2536 ± 4 mb. This measurement is the average of determinations with five different hydrocarbon samples. Special care was taken to measure neutron energy accurately throughout the experiment and to keep corrections for background and inscattering very small. The singlet effective range deduced from this measurement is 2.78 ± 0.07 fm and is consistent with values deduced from proton-proton scattering under the assumption of charge independence of nuclear forces.

I. INTRODUCTION

The importance of an accurate knowledge of the hydrogen cross section for MeV neutrons has been discussed by Breit[1] and others. This cross section is used in most neutron-flux determinations,[2] and it yields information about the nucleon-nucleon interaction. The charge dependence of the nucleon-nucleon interaction is often studied by comparing the n-p and p-p singlet effective range.[3] The calculated singlet effective range ${}^1r_{np}$ is very sensitive to the fast-neutron cross section: An error in the neutron cross section is multiplied about tenfold in the calculation of ${}^1r_{np}$.

In addition to the measured fast-neutron cross section, three other measurements are used in determining the parameters in the shape-independent approximation: the binding energy of the deuteron ϵ, the slow-neutron total cross section, and the coherent scattering length a_H. The energy ϵ is known[4] very accurately and introduces negligible uncertainty in the parameters, the slow-neutron cross section has quite recently been remeasured[5] with an accuracy of 0.1%, and a_H is believed to be known[6] with comparable accuracy. No precision measurement of the cross section for MeV neutrons has been published since 1963, although in recent years there has been much progress in experimental techniques that should permit improved accuracy in the measurements.

During the last twenty years four groups have performed precision measurements of the hydro-